Compact Self-Packaged Low-Loss SISL LPF Using Symmetric Tri-Section SIRs

Daotong Li, *Senior Member*, *IEEE*, Hao Wang, Jiaxin Wang, Ning Pan, Ying Liu, Qiang Chen, *Senior Member*, *IEEE*, and Naoki Shinohara, *Fellow, IEEE*

***Abstract*—In this paper, a compact self-packaged dc-40GHz substrate integrated suspended line (SISL) low pass filter (LPF) with the flexibly controllable cutoff frequency f_c is proposed using symmetric tri-section stepped impedance resonators (ST-SIRs). The ST-SIR structure with low pass response is investigated theoretically and numerically. Moreover, a sharp roll-off rate performance is obtained by loading the L type center-symmetric spurlines which introduces controllable multiple transmission zeros (TZs). To further enhance the stopband performance of the LPF, the defected ground structures (DGS) integrated on the SISL are demonstrated. By surrounding with metallic vias and using the shielding layer of SISL, the radiation loss can be effectively reduced. For demonstration, a LPF prototype with a maximum in-band insertion loss (*IL*) of 1.85 dB, an in-band return loss (*RL*) of more than 14.8dB, an out-of-band suppression of larger than 17.2dB (from 43GHz-67GHz), and a size of $0.41\lambda_g \times 0.69\lambda_g \times 0.44\lambda_g$ is fabricated and measured. The measured and simulated results are in good agreement.**

***Index Terms*— Compact, low loss, LPF, SISL, ST-SIRs**

I. Introduction

With the rapid development of 5G/6G communications, the demand for wideband applications surges, which puts forward more stringent requirements for mm-wave circuits today [1], [2]. In particular, low pass filters (LPFs) play a crucial role in suppressing harmonics and spurious signals in complex systems with multiple mixing and frequency multiplication stages [3]. Therefore, there is an urgent need for LPFs with compact sizes, low insertion losses, high frequency selectivity and wide stopband.

Recently, some LPFs with high performance have been reported [4-6], [10], [12]. In [5], by employing asymmetric Pi-shaped Defected Ground Structure (DGS), the low-pass filter achieved a sharp roll-off performance, but with a narrower passband range. In [8], a waveguide LPF in *X*-band with low loss and high out-of-band suppression level is proposed, but the waveguide structure is hard to integrate with other planar circuits. Commonly, step impedance resonators (SIR) [7], [8] are used to design compact filters. However, the excellent performance of SIR filters based on microstrip circuits at low frequencies will be greatly deteriorated in mm-wave bands. To comply with the requirement of high performance and integration, the type of substrate integrated lines has been widely concerned nowadays [9]. Ref. [10] demonstrates a dc-30 GHz LPF with compact size by using spoof surface plasmon polariton (SSPP) structure based on substrate integrated coaxial line (SICL), but the insertion loss (*IL*) reaches 2.1 dB. In [11], substrate-integrated suspended line (SISL) technology based on standard printed circuit board (PCB) manufacturing process is proposed. Owing to its advantages of low loss, light weight, high integration and self-packaging performance, it has been widely used in designing high performance filters [12]-[14]. In [12], an 11th-order generalized Chebyshev SISL LPF with a cutoff frequency of 18 GHz is demonstrated, which shows the possibilities of SISL in ultra-wideband circuit design. However, when designing larger bandwidth components, the method using high-order filters is relatively complex. In [13], a miniaturized SISL bandpass filter is proposed with an *IL* of 1.6 dB at *Ka*-band, which demonstrates that SISL still has an excellent performance with low loss in the mm-wave band. Choi et al. in [15] proposed a compact wide-stopband LPFs design using SIR. This design controls the frequency response by adjusting the parameters of SIRs, achieving a wide stopband and compact size, which has a clear advantage in space-limited applications. However, this wide-stopband design may increase manufacturing complexity and may be affected by material properties and manufacturing tolerances in high-frequency performance. In [16], Zhang et al. extended the filter's stopband by integrating triple-mode resonators, enhancing the filter's selectivity. This design offers more design flexibility to meet the needs of specific applications, which is a significant advantage. However, integrating multi-mode resonators may increase the difficulty of design and tuning, and there may be issues of increased cost and complexity. Bakhtiar and Al-Husseini's research [17] achieves miniaturization of LPFs

This work is supported in part by the National Key R&D Program of China under Grant No. 2018YFB1801502, in part by the National Natural Science Foundation of China under Grant 61801059, in part by the FY2021 JSPS Postdoctoral Fellowship for Research in Japan under Grant P21053, and in part by the Grant-in-Aid for JSPS Research Fellow under Grant 21F21053, in part by the Basic Research and Frontier Exploration Special of Chongqing Natural Science Foundation under Grant cstc2019jcyj-msxmX0350.

Daotong Li, Hao Wang, Ning Pan, Jiaxin Wang and Ying Liu are with School of Microelectronics and Communication Engineering, Chongqing University, Chongqing 400044, China (e-mail: dli@cqu.edu.cn).

Qiang Chen is with the Department of Communications Engineering, Tohoku University, Sendai 980-8579, Japan (e-mail: qiang.chen.a5@tohoku.ac.jp).

Daotong Li and Naoki Shinohara is the with the Research Institute for Sustainable Humanosphere, Kyoto University, Kyoto 606-8501, Japan. (e-mail: shino@rish-kyoto.ac.jp).

Color versions of one or more of the figures in this article are available online at http://ieeexplore.ieee.org.

through the use of Complementary Split-Ring Resonators (CSRRs). This design offers significant advantages in space saving and integration, particularly in mobile and portable devices. However, the CSRR design may require precise manufacturing processes to ensure the desired electromagnetic performance, which could increase production costs and complexity. Ryu et al. [18] propose a 60-GHz bandpass filter using Asymmetric Stepped-Impedance Resonators (ASIRs), providing a high-performance filtering solution for 5G applications. This design meets the high-frequency and wide bandwidth requirements of 5G technology, but it may face challenges in material loss, potentially affecting its performance across a broader frequency range. Singh et al. [19] present a Substrate Integrated Waveguide (SIW) low-pass filter integrated with a DGS, demonstrating excellent performance in millimeter-wave applications. This design effectively suppresses unwanted modes and enhances filter selectivity, but the integration of DGS may increase design complexity and sensitivity to manufacturing tolerances. Li et al. [20] offer a compact LPF design using stub-loaded resonators, maintaining good performance while achieving miniaturization. However, the design of stub-loaded resonators may require precise dimensional control to ensure the filter's correct resonance, which could limit design flexibility. Kim et al. [21] propose a dual-band low-pass filter design that achieves dual-frequency filtering through asymmetric loading technology, potentially advantageous in multi-frequency applications. However, this design may require a complex tuning process to ensure filtering performance across both frequency bands, increasing the difficulty in design and manufacturing.

In this paper, a dc-40 GHz LPF by using symmetric tri-section stepped impedance resonators (ST-SIRs) based on self-packaged SISL platform is proposed. The cutoff frequency f_c can be flexibly adjusted by changing the physical sizes of the ST-SIRs. To improve the frequency selectivity of the LPF, a pair of center-symmetric L-type spurlines is loaded on SISL transmission line, which introduces additional transmission zeros (TZs) near the passband side and realizes a sharp roll-off skirt performance. The DGSs are loaded on top and bottom substrates of SISL to further broaden the stopband performance. The detailed analysis and design are in section II. Manufactured prototype and measured results are in section III.

II. Analysis and Design of the SISL LPF

As shown in Fig. 1, the proposed SISL LPF consists of a five-layer dielectric substrate. The top and bottom surfaces of each dielectric substrate are covered with copper layers (G1-G10). With the exception of Sub3, which uses Rogers 5880 (with h_3 = 0.254mm, ε_r = 2.2, tanδ_d = 0.0009), the other layers are low cost FR4 substrates (with $h_1 = h_2 = h_4 = h_5$ = 0.4mm, ε_r = 4.4, tanδ_d = 0.02). Sub2 and Sub4 are hollowed out to form air cavities, with the cavity width a = 3.5 mm, length b = 1.5 mm, and height H = $h_2 + h_3 + h_4$. Sub1 and Sub5 construct effective electromagnetic (EM) shielding boundaries. The suspended line circuit is mainly laid on copper layer G5. DGS structures are symmetrically integrated on copper layer G2 ang G10, respectively.

A. Analysis of symmetrical tri-section SIRs

The proposed LPF circuit structure with loaded ST-SIRs based on SISL platform is shown in Fig. 2(a). Two λ/4 tri-section SIRs are symmetric about the y-axis, which are loaded on a horizontal inductance suspended line to achieve low pass response. As illustrated in Fig. 2(b), the tri-section SIR consists of three transmission lines with electrical lengths θ_1, θ_2, and θ_3, and the corresponding impedances are Z_1, Z_2, and Z_3, respectively. According to Ref. [22], [23], the input impedance Z_{in} of the tri-section SIR can be expressed as:

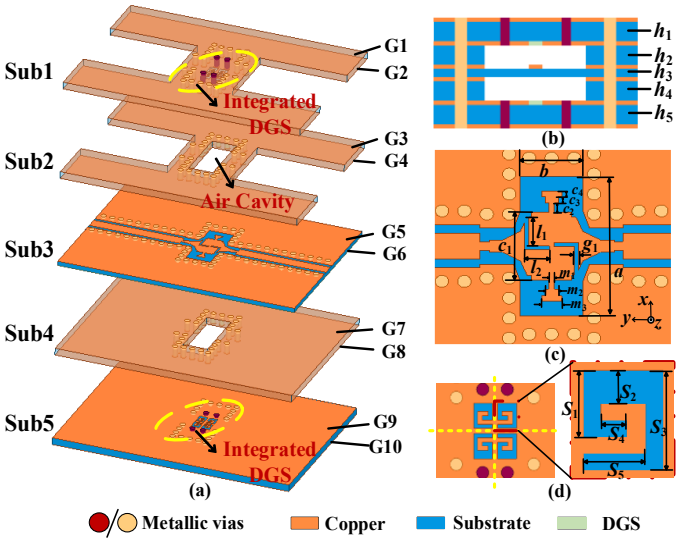

Fig. 1. Structure of the proposed LPF based on SISL platform. (a) 3D view, (b) cross view, (c) main circuit on Sub3, (d) details of the integrated DGS structure.

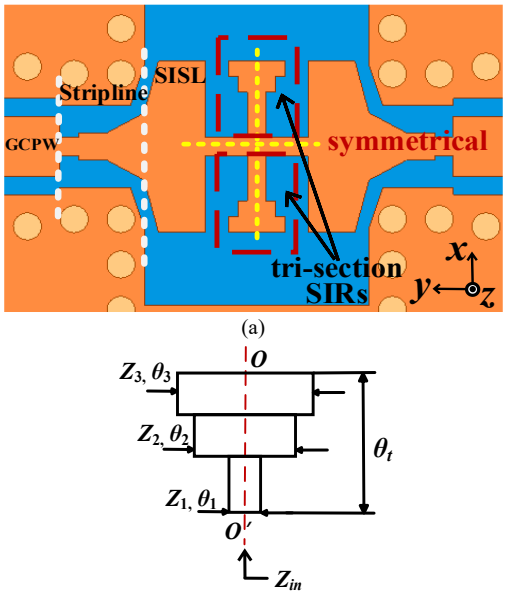

Fig. 2. (a) Original circuit of LPF loading ST-SIRs, and (b) geometry of λ/4 tri-section SIR.

$$Z_{in} = jZ_2 \frac{-K_1 + \tan\theta_2 \tan\theta_3 + \frac{\tan\theta_1}{K_2}(\tan\theta_3 + K_1 \tan\theta_2)}{\tan\theta_3 + K_1 \tan\theta_2 + K_1 K_2 \tan\theta_1 - K_2 \tan\theta_1 \tan\theta_2 \tan\theta_3} \quad (1)$$

where $K_1=Z_3/Z_2$, $K_2=Z_2/Z_1$ represent impedance ratios.

To simplify the analysis, $\theta_1=\theta_2=\theta_3=\theta$ of the tri-section SIR has been set. When it is resonant, the expression between θ, the resonance frequencies (f_1, f_2, f_3) and the impedance ratios (K_1, K_2) can be derived as:

$$\theta = \tan^{-1}\left(\sqrt{\frac{K_1 K_2}{K_1 + K_2 + 1}}\right) \tag{2}$$

$$K_1 = \frac{Z_3}{Z_2} = \frac{\tan^2\left(\frac{\pi}{2}\frac{f_1}{f_3}\right)\left[1+\tan^2\left(\frac{\pi}{2}\frac{f_2}{f_3}\right)\right]}{1+\tan^2\left(\frac{\pi}{2}\frac{f_1}{f_3}\right)} \tag{3}$$

$$K_2 = \frac{Z_2}{Z_1} = \frac{K_1+1}{\tan^2\left(\frac{\pi}{2}\frac{f_2}{f_3}\right)-K_1} \tag{4}$$

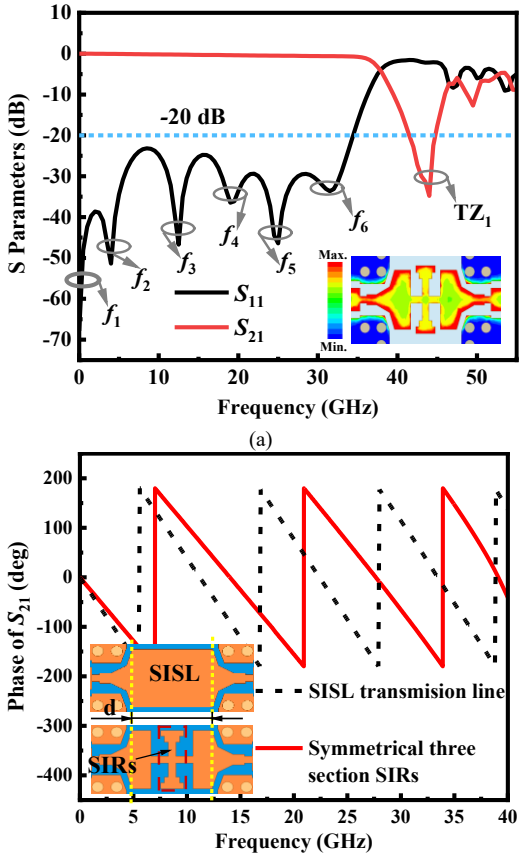

Fig. 3. (a) The low pass filtering response of symmetric tri-section SIRs, and (b) slow wave properties of ST-SIRs.

According to formulas (1)-(4), it can be known the resonant frequencies can be flexibly controlled by adjusting the physical size of tri-section SIR. For ST-SIRs, the total electrical length $\theta_{st} = \theta_t = 2(\theta_1+\theta_2+\theta_3)$ [22], which corresponds to six resonant frequencies f_i (i = 1,2,3…6) as depicted in Fig. 3(a). And the ST-SIRs demonstrate a substantial low pass filtering response in Fig3(a). From Fig. 3(b), it's evident that compared to SISL transmission lines with the same length (d = 2mm), the ST-SIRs exhibit pronounced slow wave characteristics. It enables a more compact size for the device by adjusting the ST-SIRs' parameters. Moreover, some key parameters affecting the cutoff frequency f_c of LPF are also investigated numerically.

As illustrated in Fig. 4(a), it's apparent that when the parameter c_2 is varied from 1.2mm to 0.6mm, the cut-off frequency f_c shifts towards higher frequencies. Similarly, in Fig. 4(b), as the parameter m_3 changes from 1.1mm to 0.5mm, the cut-off frequency f_c also moves towards higher frequencies. It demonstrates that the proposed ST-SIRs LPF has flexibly controllable cut-off frequency.

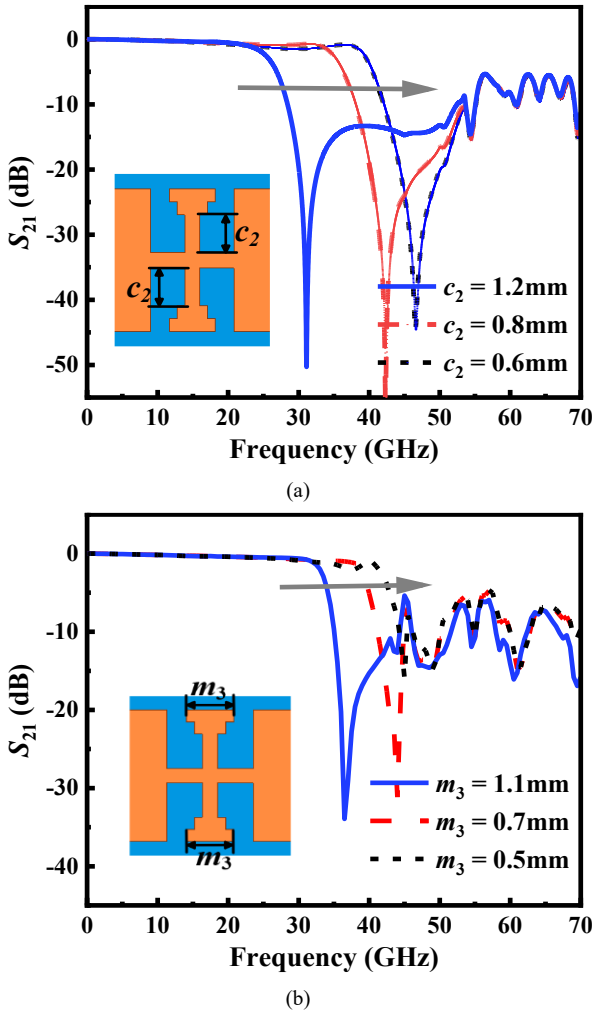

Fig. 4. Parameters affecting the cutoff frequency f_c of ST-SIRs LPF. (a) simulated S_{21} variations versus c_2 and (b) simulated S_{21} variations versus m_3.

B. Center-symmetric spurlines and DGS integrated on SISL

To further enhance the frequency selectivity of the filter, a pair of center-symmetric L-type spurlines are incorporated into the proposed LPF structure in subsection A, as illustrated in Fig. 5(a). The spurline resonator can be equivalent to a parallel RLC resonant circuit because of its bandgap property [24], as demonstrated in Fig. 5(b). The slotted gap capacitance is equivalent to the capacitance C of the resonator, while the slot line can be approximated as an inductance L of the resonator.

Moreover, the current vector ***J*** distribution of the LPF with loaded center-symmetric spurlines is shown in Fig. 5(c). It is evident that by employing two center-symmetric spurlines, named spurline ① and spurline ②, two current paths rotating counterclockwise and clockwise, respectively, are introduced, which create multiple TZs close to the passband as shown in Fig. 6.

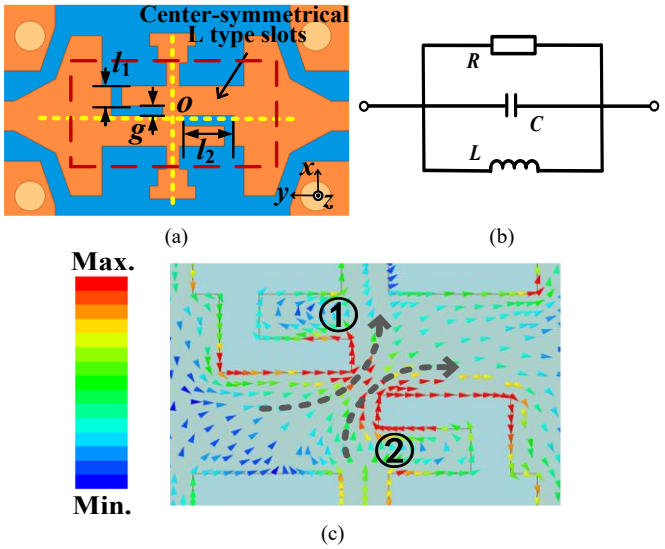

Fig. 5. (a) Geometry of center-symmetric spurlines, (b) equivalent circuit of spurlines, and (c) current vector ***J*** distributions of center-symmetric spurlines.

Notably, the incorporation of center-symmetric spurlines results in a sharp roll-off performance, the roll-off rate (S_{21} from -3dB to -20dB) is improved nearly 10 times compared to the original structure in Fig. 2(a). It is worth noting that the lengths (l_1 and l_2) and the gap width (g_1) of the spurlines are the key impact parameters. Consequently, the TZs outside the passband and the roll-off rate of the LPF can be flexibly tuned by changing the lengths l_1 and l_2 of the spurlines as investigated in Fig. 7. It can be seen from Fig. 7(a) that as the parameter l_1 varies from 0.1mm to 0.3mm, TZ_1 gradually moves away from the passband side and towards higher frequencies, while TZ_3 moves towards lower frequencies, exhibiting a deeper out-of-band rejection level. Similarly, as depicted in Fig. 7(b), when the parameter l_2 varies from 0.5mm to 0.7mm, all the TZs gradually approach the passband side, accompanied by an increased out-of-band rejection. Consequently, the frequency selectivity of the LPF can be effectively improved by flexibly controlling the position of the TZs.

The stopband performance is another important performance of LPF. It can be seen that the bandwidth of stopband is only ranging from 40.2 to 45.5 GHz. By cascading multiple DGS units to broaden the stopband of filters in microstrip circuits has been commonly used [5]. However, it will not only increase the size of the components, but also the radiation loss will increase greatly because the ground is destroyed, especially in mm-wave frequency. The substrate integrated defected ground structure (SIDGS) [25] has been reported recently as an effective method to reduce radiation loss due to DGS. Inspired by SIDGS and combining the advantages of high design freedom of multi-layer and self-shielded characteristics of SISL, two pairs of DGS structures are symmetrically integrated on layer G2 and G10 of SISL, as shown in Fig. 1(a) and (d), respectively.

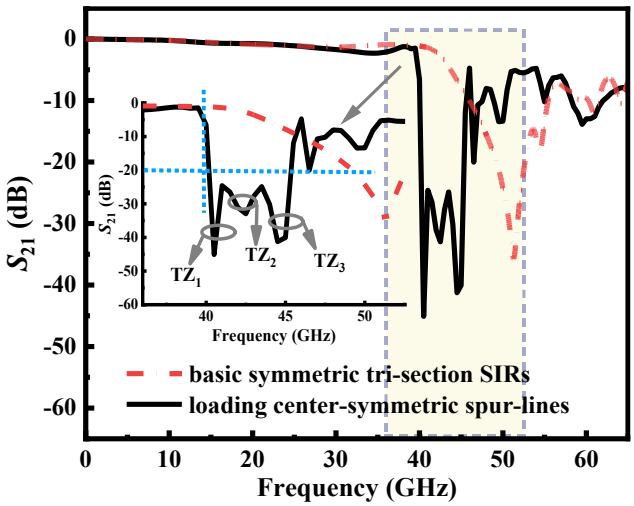

Fig. 6. Comparison of S_{21} with and without center- symmetric spurlines.

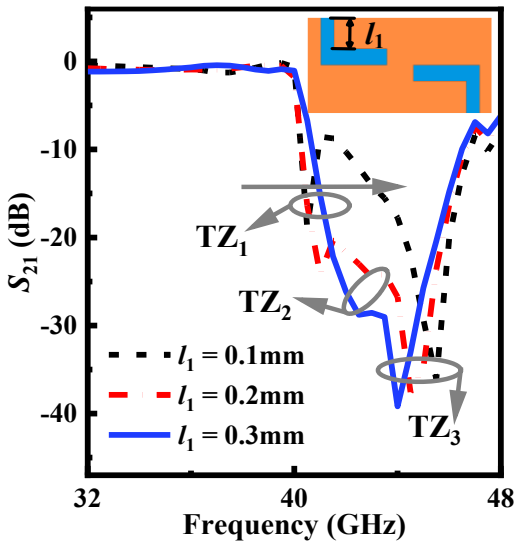

(a)

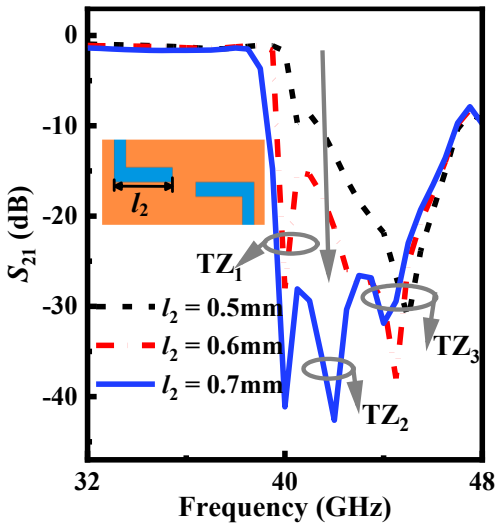

(b)

Fig. 7. Simulated S_{21} variations versus (a) parameter l_1, and (b) parameter l_2.

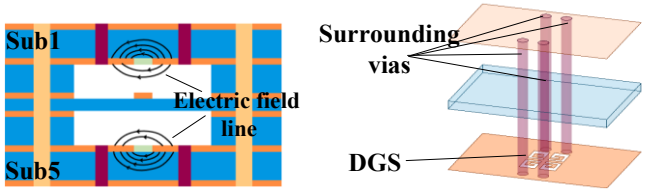

(a)

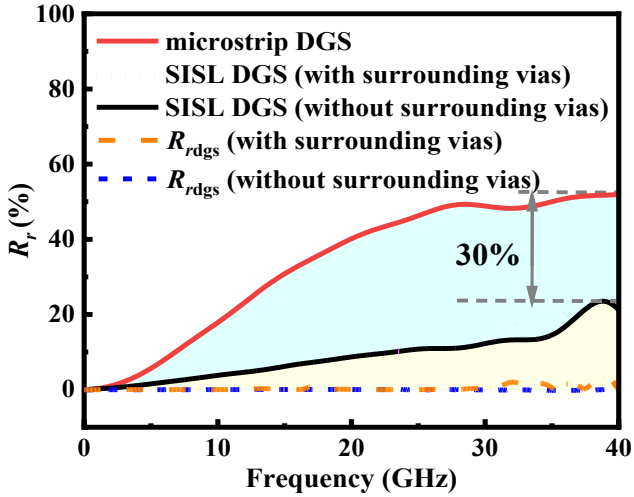

(b)

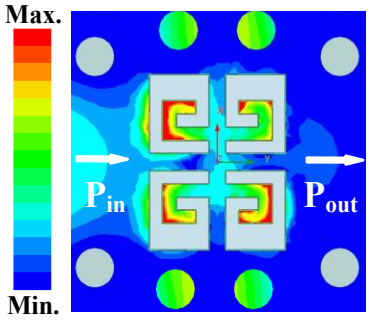

(c)

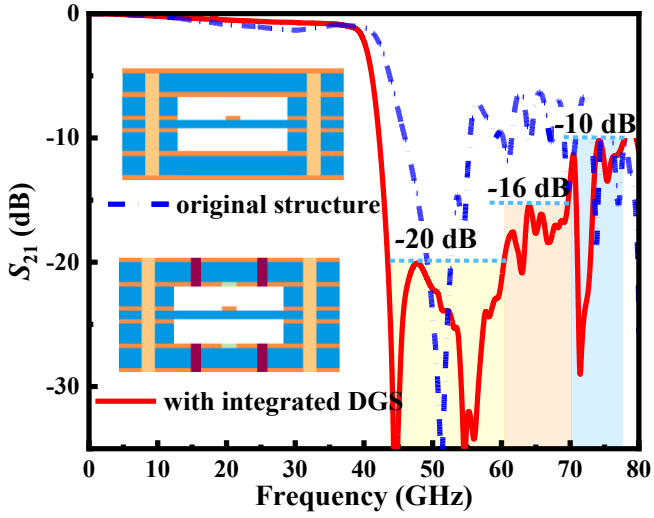

(d)

Fig. 8. (a) Structure of DGS shielded by metallic vias, (b) simulated results of radiation R_r, (c) E-field distribution diagram at 65GHz, and (d) simulated of S_{21} about stopband when compared to original structure.

It can be seen from Fig. 8(a) that DGS shielded by surrounding metallic vias and metal layer G1(G10) can confine the electric field lines between DGS and ground. And the metallic vias around DGS throughout Sub1 and Sub5 are used to prevent dissipation into the substrate. Since the radiation loss R_r can be calculated by the formula $R_r = 1-|S_{11}|^2-|S_{21}|^2$, which of SISL DGS (including the transition section from GCPW to SISL) is significantly reduced as shown in Fig. 8(b), especially the maximum R_r is reduced by 30% when compared to microstrip DGS. Furthermore, depending on the self-packaged characteristic of SISL, the radiation loss R_{rdgs} introduced only by the DGS tends to zero (excluding the GCPW-SISL transition section) as shown in Fig8(b), which confirms that integrating DGS on SISL can effectively reduce the radiation loss. It can be seen from the EM field distribution diagram at 65GHz in Fig.8(c) that four symmetrical "G-type" DGS cells integrated on the metal layer M2(M9) of SISL can effectively suppress the out-of-band stray resonance frequencies. Thus, the simulated stopband is finally extended to 60 GHz with S_{21} of -20 dB and further to 70 GHz with S_{21} of -16 dB when DGS structures are integrated on SISL as illustrated in Fig. 8(d).

III. LPF Manufacturing, Packaging and Measurement

The prototype of LPF is manufactured based on standard PCB process as shown in Fig. 9(a) and (b), and the physical size of the cavity is $0.41\lambda_g \times 0.69\lambda_g \times 0.44\lambda_g$, where λ_g represents the guided wavelength at 40GHz. The GCPW is employed as interface to carry out measurement based on our previous work on the GCPW to SISL transition structure [26]. Finally, the filter assembled with 2.92mm connectors, as illustrated in Fig. 9(c), is measured by R&S®ZNA67 vector network analyzer.

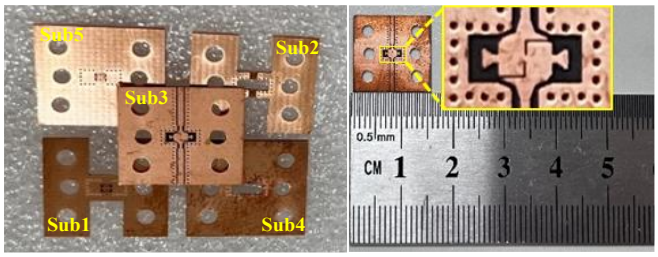

(a) (b)

(c)

Fig. 9 Prototype of proposed LPF. (a) Whole structure, (b) details of LPF on Sub3, (c) assembly diagram. (a = 3.5mm, c_1 = 1.69mm, c_2 = 0.23mm, c_3 = 0.17mm, c_4 = 0.13mm, m_1 = 0.13mm, m_2 = 0.29mm, m_3 = 0.45mm, l_1 = 0.72mm, l_2 = 0.55mm, g_1 = 0.1mm, l_2 = 0.55mm, s_1 = 0.4mm, s_2 = 0.2mm, s_3 = 0.6mm, s_4 = 0.15mm, s_4 = 0.36mm).

It can be seen form Fig. 10 (a), the measured in-band *IL* of the LPF is no more than 1.85 dB from dc to 40 GHz and the measured in-band *RL* is better than 14.8 dB. The measured stopband with -17.2 dB rejection varies from 43GHz to 67GHz. For ultra-wideband filters applied in communication systems, a flat group delay is necessary because significant group delay varying with frequency have a dispersion effect on the signal [12]. As shown in Fig. 10(b), the measured group delay τ_g of the LPF in the passband is no more than 0.5 ns and relatively flat, which is in good agreement with the simulation ones. The inconsistencies between the simulated and measured results mainly caused by additional losses introduced by launch connectors, fabricating accuracy error and experimental assembly errors.

Table I
COMPARISON WITH OTHER PREVIOUS WORKS

Ref.	Technology	f_c (GHz)	*IL* (dB)	*RL* (dB)	Size (λ_g^3)	R. C.	OS (dB)	SB (GHz)	Substrates	Self-packaging
[5]	Microstrip[#1]	dc-1	<2	>12	0.00038	1.2*	>30	1.6-6.5*	PET	No
[6]	Waveguide	10.3-12.6	<0.4	>15	5.09	1.02*	>60	13.7-43*	WR75	Yes
[10]	MCSICL[#2]	dc-30	<2.1	>10	0.42	1.17*	>35	36-60*	Rogers 5880	Yes
[12]	SISL	dc-18	<1	>12	0.282	1.07*	>30	19-26	Rogers 6002/6006	Yes
[13]	SISL	27.7-30.7	<1.6	>17	0.122	2	>80	35-65*	FR4	Yes
This work	**SISL**	**dc-40**	**<1.85**	**>14.8**	**0.124**	**1.09**	**>17.2**	**43-67**	FR4/ Rogers 5880	Yes

Ref.: reference, f_c: cutoff frequency, R. C.: Rectangular Coefficient = $|BW_{-30dB}/BW_{-3dB}|$, OS: out-of-band suppression, SB: upper stopband, #1: microstrip based on polyimide film substrate, #2: condition of low pass part, *: estimated value from figures.

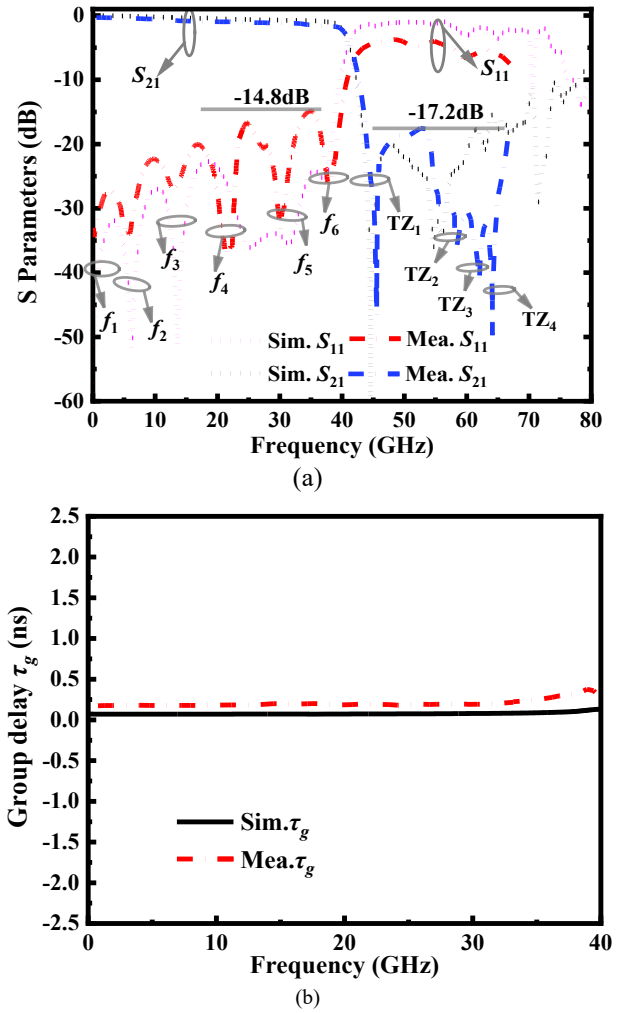

Fig. 10 Simulated and measured results of the proposed LPF. (a) *S* parameters of S_{11} and S_{21}, and (b) group delay τ_g.

Table I shows the comparison of the proposed works with some typical works. Compared with the LPFs in Refs. [5], [6], [10], [12], the proposed LPF has the advantages of low loss and compact size. Compared to the bandpass filter in Ref. [13] which also excels in terms of *IL* and size, the proposed work has advantages in the aspect of operating bandwidth wider from dc-40 GHz and sharp roll-off skirt.

IV. CONCLUSION

In this brief, a dc-40 self-packaged compact GHz SISL LPF using ST-SIRs with low loss is proposed. The resonant characteristics of ST-SIRs are analyzed, and the cutoff frequency f_c can be adjusted flexibly by changing the physical sizes of ST-SIRs. Moreover, controllable TZs are introduced near the passband side to improve the frequency selectivity of the LPF by loading center-symmetric spurlines. The top and bottom shielding layers of SISL are also utilized to enhance the stopband of the LPF by integrating DGS structures. It is worth noting that utilizing the multi-layer characteristics of SISL to achieve multifunctional complex circuits may be a feasible trend. The proposed LPF is fabricated and measured, which is suitable for mm-wave communication applications requiring large bandwidth and high integration.

REFERENCE

[1] K. Hu, T. W. Callis and M. M. Tentzeris, "Additively Manufactured Flexible On-Package Phased Antenna Arrays With Integrated Microfluidic Cooling Channels for 5G/mmWave System-on-Package Designs," *IEEE Microwave and Wireless Technology Letters*, vol. 33, no. 6, pp. 899-902, June 2023.

[2] H. Tian and Y. Dong, "Wideband Low-Loss Filter With Compact Size

and Wide Stopband Based on Folded Planar Waveguide," *IEEE Microwave and Wireless Technology Letters*, vol. 33, no. 6, pp. 651-654, June 2023.

[3] K. Ma, S. Mou, K. S. Yeo and W. M. Lim, "A Cross-Coupled LPF Topology and Design for Millimeter-Wave RFIC Applications," *IEEE Transactions on Electron Devices*, vol. 59, no. 11, pp. 2902-2909, Nov. 2012.

[4] J. Xu, Y. -X. Ji, W. Wu and C. Miao, "Design of Miniaturized Microstrip LPF and Wideband BPF With Ultra-Wide Stopband," *IEEE Microwave and Wireless Components Letters*, vol. 23, no. 8, pp. 397-399, Aug. 2013.

[5] Z. -h. Liu, Y. -n. Han, X. -b. Qiu and X. -l. Li, "A Novel Translucent Lowpass Filter Design Using Asymmetric Pi-shaped DGS," 2023 IEEE 7th International Symposium on Electromagnetic Compatibility (ISEMC), Hangzhou, China, 2023, pp. 1-3.

[6] M. Yang et al., "Design of Wide Stopband for Waveguide Low-Pass Filter Based on Circuit and Field Combined Analysis," *IEEE Microwave and Wireless Components Letters*, vol. 31, no. 11, pp. 1199-1202, Nov. 2021.

[7] H. Liu, T. Liu, Q. Zhang, B. Ren and P. Wen, "Compact Balanced Bandpass Filter Design Using Asymmetric SIR Pairs and Spoof Surface Plasmon Polariton Feeding Structure," *IEEE Microwave and Wireless Components Letters*, vol. 28, no. 11, pp. 987-989, Nov. 2018.

[8] A. Sheikhi, A. Alipour and A. Mir, "Design and Fabrication of an Ultra-Wide Stopband Compact Bandpass Filter," *IEEE Transactions on Circuits and Systems II: Express Briefs*, vol. 67, no. 2, pp. 265-269, Feb. 2020.

[9] K. Wu, M. Bozzi and N. J. G. Fonseca, "Substrate Integrated Transmission Lines: Review and Applications," *IEEE Journal of Microwaves*, vol. 1, no. 1, pp. 345-363, Jan. 2021.

[10] Y. Zhu, X. -C. Li and J. -F. Mao, "Mode Composite Substrate Integrated-Coaxial Line Based on Substrate Integrated Coaxial Line and Periodic L-Shaped SSPP Structure," *IEEE Transactions on Components, Packaging and Manufacturing Technology*, vol. 13, no. 4, pp. 528-536, April 2023.

[11] K. Ma and K. T. Chan, "Quasi-planar circuits with air cavities," WO Patent WO/2 007 149 046, Dec. 27, 2007.

[12] J. W. McDaniel, S. Saeedi, M. B. Yeary and H. H. Sigmarsson, "A Low-Loss Fully Board-Integrated Low-Pass Filter Using Suspended Integrated Strip-Line Technology," *IEEE Transactions on Components, Packaging and Manufacturing Technology*, vol. 8, no. 11, pp. 1948-1955, Nov. 2018.

[13] Z. Yue, K. Ma and Y. Wang, "Design of Ka-Band SISL High Selectivity Bandpass Filter With Controllable Zeros," *IEEE Microwave and Wireless Technology Letters*, vol. 33, no. 9, pp. 1278-1281, Sept. 2023.

[14] Y. Ding, K. Ma, Y. Wang, N. Yan, Y. Wu and F. Feng, "Novel Miniaturized Self-Packaged Filters Based on Metasubstrate in SISL Platform," *IEEE Transactions on Circuits and Systems II: Express Briefs*, vol. 70, no. 8, pp. 2879-2883, Aug. 2023.

[15] J.-H. Choi, S.-W. Yun, and B.-W. Min, "A Compact and Wide-Stopband Low-Pass Filter Using Stepped-Impedance Resonators," *IEEE Transactions on Microwave Theory and Techniques*, vol. 69, no. 10, pp. 4220-4229, Oct. 2021.

[16] L. Zhang, Y.-J. Zhang, and X.-W. Shi, "Design of a Low-Pass Filter With Integrated Triple-Mode Resonators for Wide Stopband," *IEEE Transactions on Circuits and Systems II: Express Briefs*, vol. 69, no. 12, pp. 4343-4347, Dec. 2022.

[17] M. H. Bakhtiar and M. A. Al-Husseini, "Design of a Miniaturized Low-Pass Filter Using Complementary Split-Ring Resonators," *IEEE Microwave and Wireless Components Letters*, vol. 32, no. 12, pp. 1136-1138, Dec. 2022.

[18] J.-H. Ryu, S.-W. Yun, and B.-W. Min, "A 60-GHz Bandpass Filter With Asymmetric Stepped-Impedance Resonators for 5G Applications," *IEEE Transactions on Terahertz Science and Technology*, vol. 12, no. 3, pp. 378-386, May 2022.

[19] A. K. Singh, S. K. Mishra, and S. K. Koul, "Substrate Integrated Waveguide (SIW) Low-Pass Filter With Defected Ground Structure (DGS) for Millimeter-Wave Applications," *IEEE Transactions on Components, Packaging and Manufacturing Technology*, vol. 11, no. 7, pp. 1157-1165, July 2021.

[20] X. Li, T. Wang, and Y. Fan, "Design and Analysis of a Compact Low-Pass Filter Using Stub-Loaded Resonators," *IEEE Transactions on Circuits and Systems II: Express Briefs*, vol. 68, no. 12, pp. 4148-4152, Dec. 2021.

[21] H.-T. Kim, J.-H. Choi, and B.-W. Min, "A Dual-Band Low-Pass Filter With Asymmetrically Loaded Stepped-Impedance Resonators," *IEEE Microwave and Wireless Components Letters*, vol. 32, no. 3, pp. 220-222, Mar. 2022.

[22] D. Packiaraj, M. Ramesh and A. T. Kalghatgi, "Design of a tri-section folded SIR filter," *IEEE Microwave and Wireless Components Letters*, vol. 16, no. 5, pp. 317-319, May 2006.

[23] A. M. Salem, H. N. Ahmed, E. K. Abouseif and M. A. Elkfafy, "A highly selective, tri-band BPF using tri-section SIR with wideband harmonic suppression," 2017 Japan-Africa Conference on Electronics, Communications and Computers (JAC-ECC), Alexandria, Egypt, 2017, pp. 65-68.

[24] H. Shaman and J. -S. Hong, "Ultra-Wideband (UWB) Bandpass Filter With Embedded Band Notch Structures," *IEEE Microwave and Wireless Components Letters*, vol. 17, no. 3, pp. 193-195, March 2007.

[25] D. Tang, C. Han, Z. Deng, H. J. Qian and X. Luo, "Substrate-Integrated Defected Ground Structure for Single- and Dual-Band Bandpass Filters With Wide Stopband and Low Radiation Loss," *IEEE Transactions on Microwave Theory and Techniques*, vol. 69, no. 1, pp. 659-670, Jan. 2021.

[26] J. Wang, D. Li, L. Shi, L. Zhang, X. Chen and Q. Chen, "A DC-40 GHz Substrate Integrated Suspended Line (SISL) to GCPW Transition," *2023 International Conference on Microwave and Millimeter Wave Technology (ICMMT)*, Qingdao, China, 2023, pp. 1-3.

Daotong Li (Senior Member, IEEE) received the Ph.D. degree in electromagnetic field and microwave technology from the University of Electronic Science and Technology of China, Chengdu, China, in 2016. He is currently with the Center of Tracking Telemetry Command, Chongqing University, Chongqing.

He has been a Visiting Researcher with the Department of Electrical and Computer Engineering, University of Illinois at Urbana-Champaign from 2015 to 2016, later joining Chongqing University as Assistant Professor in 2017 and being promoted to Associate Professor in 2019. His academic journey includes being awarded a JSPS Fellowship at Tohoku University from Nov.2021 to Nov. 2023, and serving as a visiting associate professor at Kyoto University in 2024, and being a Guest Scholar since June 2024. His research focuses on RF/microwave/millimeter-wave technologies, microwave power transmission (MPT), and antennas, with over 100 peer-reviewed publications. His achievements include receiving the UESTC Outstanding Graduate Awards (2016), National Graduate Student Scholarship, and "Tang Lixin" Scholarship. His professional service includes reviewing for IEEE/IET journals and participating in international conferences as TPC Member, Session Organizer and Chair..

Hao Wang received the B.S. degree in South-Central Minzu University, China, in 2023. He is currently pursuing the M.S. degree in Electronic Information with the School of Microelectronics and Communication Engineering, Chongqing University, China.

His current research interests include microwave circuits and systems.

Jiaxin Wang

Ying Liu received the M.S. degree in communication and information system from the Chongqing University, Chongqing, China, in 2015. She is currently with the College of Microelectronics and Communication Engi-neering, Chongqing University, Chongqing. Her research focuses on microwave photonics and image processing.

Qiang Chen received the B.E. degree from Xidian University, Xi'an, China, in 1986, the M.E. and D.E. degrees from Tohoku University, Sendai, Japan, in 1991 and 1994, respectively. He is currently Chair Professor of Electromagnetic Engineering Laboratory with the Department of Communications Engineering, Faculty of Engineering, Tohoku University. His primary research interests include antennas, microwave and millimeter wave, electromagnetic measurement, and computational electromagnetics.

He received the Best Paper Award and Zen-ichi Kiyasu Award from the Institute of Electronics, Information and Communication Engineers (IEICE). He served as the Chair of IEICE Technical Committee on Photonics-applied Electromagnetic Measurement from 2012 to 2014, the Chair of IEICE Technical Committee on Wireless Power Transfer from 2016 to 2018, the Chair of IEEE Antennas and Propagation Society Tokyo Chapter from 2017 to 2018, the Chair of IEICE Technical Committee on Antennas and Propagation from 2019 to 2021. IEICE Fellow.

Naoki Shinohara (Fellow, IEEE) received the Ph.D. degree in electrical engineering from the Kyoto University, Kyoto, Japan, in 1996. He is currently a Professor with the Research Institute for Sustainable Humanosphere, Kyoto University, Kyoto.

He has been affiliated with Kyoto University since 1996, becoming a Professor in 2010, where he conducts pioneering research on solar power satellites and microwave power transmission systems. He has authored seminal works including Wireless Power Transfer via Radiowaves (Wiley, 2014) and edited several authoritative volumes on wireless power technologies. An IEEE Distinguished Microwave Lecturer (2016-2018) and current IEEE AdCom Member (2022-2024), Dr. Shinohara plays multiple leadership roles across prestigious organizations: he founded the IEEE Wireless Power Transfer Conference and serves on its Steering Committee, chairs URSI Commission D and the Wireless Power Transfer Consortium for Practical Applications (WiPoT), acts as Executive Editor for the International Journal of Wireless Power Transfer, and holds vice-chairmanship of the Space Solar Power Systems Society. His extensive committee engagements span IEEE MTT-S Technical Committee 25, IEICE Wireless Power Transfer, and various Japanese research consortia, cementing his status as a global leader in advancing wireless power technologies.